COMMUNICATION

Check for updates

The temperature dependence of Mössbauer quadrupole splitting values: a quantum chemical analysis†

Niklas von Rhein [ID] and Vera Krewald [ID]*

The two key parameters extracted from Mössbauer spectroscopy, isomer shift and quadrupole splitting, have well-known temperature dependencies. While the behavior of the values following a temperature change has long been known, its microscopic origins are less clear. For quantum chemical calculations – formally representing the situation at 0 K – significant discrepancies with the experiment can arise, especially at elevated temperatures. Herein, we introduce an ensemble-based approach for capturing the temperature dependence of the quadrupole splitting. Our method is exemplified with [Fe(TPP)(2-MeHIm)], an iron(II) high spin system. We rationalise the temperature dependence by changes in the shape of the charge distribution due to vibrational distortion. By using a normal mode fitting approach, we isolated collective nuclear movements associated with the change in the quadrupole splitting.

Mössbauer spectroscopy is a key method for investigating structural and electronic properties of iron nuclei in molecular environments,[1] *e.g.* bioinorganic systems like hemoglobin, P450, and nitrogenase,[2–7] molecular complexes and catalysts,[8–14] or single atom catalysts[15–18] such as FeNC catalysts for the oxygen reduction reaction.[19–26] Mössbauer spectroscopy is often used to elucidate structures and electronic structures, usually in combination with density functional theory calculations on known or plausible systems.[27–35] While Mössbauer spectroscopy—like many other spectroscopies—shows a temperature dependence,[11,12,36–38] quantum chemical calculations are usually restricted to a rigid equilibrium geometry at absolute zero.[39] For Mössbauer spectroscopy, this limits the direct comparison of experiment and theory to experimental temperatures below *ca.* 80 K, and makes the assignment of signals observed under *in situ* or *operando* conditions at higher temperatures significantly less reliable.

The two key Mössbauer parameters, isomer shift and quadrupole splitting (see Fig. 1), are altered by several temperature-dependent effects,[1] such as the second-order Mössbauer effect on the isomer shift.[1,40,41] An effect that may influence both isomer shift and quadrupole splitting is that different electronic states may be thermally accessible at a given temperature due to the energetic proximity of different configurations or multiplicities, or due to even smaller energy gaps introduced by spin–orbit coupling. These effects are exploited in spin crossover complexes.[42–49]

Herein, we focus on an effect that mainly influences the quadrupole splitting: the influence of vibrational movements of a molecular complex that are inherently temperature-sensitive.

The quadrupole splitting and its sign depend on the shape of the charge distribution around the iron nucleus. The electric field gradient tensor (EFG) has diagonal components $|V_{zz}| \geq |V_{yy}| \geq |V_{xx}|$. If $|V_{zz}| \gg |V_{yy}|$, a positive sign of the quadrupole splitting indicates an oblate charge distribution, while a negative sign corresponds to a prolate one. Even from basic crystal field theory considerations it is clear that the EFG will be influenced by the ligand field splitting.[1] Vibrational movements will influence the charge distribution as well as the ligand field splitting and consequently the magnitude and shape of the EFG. Since the macroscopic measurement probes the superposition of all vibrationally accessible structures, the observed quadrupole splitting is expected to be sensitive to the temperature.
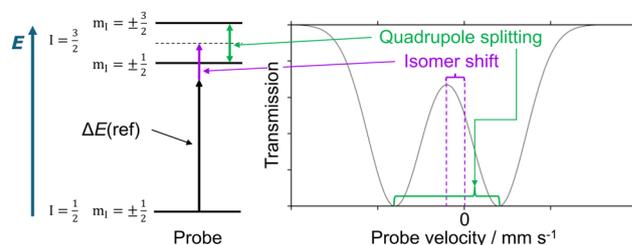
Fig. 1 Right: Exemplary Mössbauer doublet signal plotted as transmission *vs.* probe velocity. The isomer shift (violet) refers to the center of the doublet with respect to a reference (typically, α-iron). The quadrupole splitting (green) measures the separation of the doublet minima. Left: Diagram with the nuclear energy levels; labels refer to the nuclear spin quantum number I and the nuclear magnetic quantum number m_I.

Department of Chemistry, Quantum Chemistry, TU Darmstadt, Peter-Grünberg-Str. 4, 64287 Darmstadt, Germany. E-mail: vera.krewald@tu-darmstadt.de

To the best of our knowledge, the influence of vibrational distortions on Mössbauer parameters has not yet been evaluated in a quantum chemical study. Our approach is to generate an ensemble representative for a given temperature using Wigner sampling.[50–52] This allows us to study the temperature-dependence of the quadrupole splitting explicitly for the first time. Moreover, our analysis provides possible explanations for the experimental observations that are rooted in an electronic structure and normal mode analysis of the ensemble.

Our approach requires three steps as described briefly in the following; details are given in the ESI.† All quantum chemical calculations were performed using the ORCA 5.0 program suite (see ESI,† Method S1).[53–55] (1) A DFT geometry optimization and frequency calculation is carried out; here, TPSS/def2-TZVP:def2-SVP (heteroatoms: carbon, hydrogen) is chosen as the theory level.[56–58] (2) Using Wigner sampling[50,51] as implemented in the SHARC program,[59,60] an ensemble of displaced structures is created that is representative for a given temperature (see ESI,† Method S2); here, 600 structures are generated per temperature of interest (see ESI,† Fig. S1, for convergence behaviour). In contrast to MD-based approaches, Wigner sampling uses the harmonic approximation and takes into account zero-point energies.[61] (3) For all structures in the ensemble, the Mössbauer parameters are calculated using DFT; here, in accordance with a previous calibration study,[27] B3LYP/CP(PPP):def2-TZVP (iron:all other atoms) is chosen as the theory level.[58,62,63] This theory level has uncertainties of ± 0.13 mm s^{-1} and ± 0.22 mm s^{-1} for the isomer shift and the quadrupole splitting, respectively, as determined by an in-house calibration study following the work of Gallenkamp et al.[27] using ORCA 5.0 instead of ORCA 4.2 (see ESI,† Method S1).

To test our approach, we chose the Fe(II) high spin complex [Fe(TPP)(2-MeHIm)], see Fig. 2. Its experimental Mössbauer parameters are taken from ref. 11, see Table 1.[11,12] Fe(II) high spin complexes are advantageous as they have exceptionally high isomer shifts which are easily discernible from other spin and oxidation states.[1] While iron is notorious for its complicated electronic structure, which often renders it challenging for DFT as a single-determinant method,[64–67] the large number of single point calculations per ensemble required DFT as an efficient computational method. The high spin state of [Fe(TPP)(2-MeHIm)] was identified as the ground state (see ESI,† Table S1, for spin state energies). The Mössbauer parameters for the equilibrium structure are $\delta = 0.94$ mm s^{-1} and $\Delta E_Q = 2.84$ mm s^{-1}, in good to reasonable agreement with the experiment. We note that
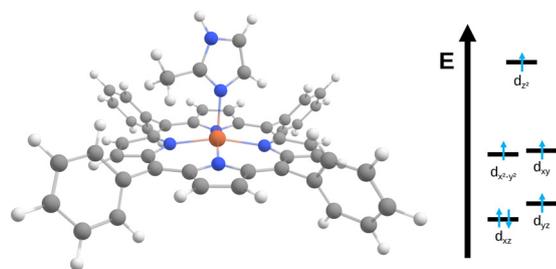
Table 1 Experimental and calculated Mössbauer parameters of [Fe(TPP)(2-MeHIm)] at different temperatures; in "calculations (all)", the Mössbauer parameters are averaged over all members of the ensemble, in "calculations (filtered)" the Mössbauer parameters are only averaged over structures with a $d_{x^2-y^2}(\beta)$ orbital occupation $<32\%$

	Experiment		Theory (all)		Theory (filtered)	
T/K	$\delta/$ mm s^{-1}	$\Delta E_Q/$ mm s^{-1}	$\delta/$ mm s^{-1}	$\Delta E_Q/$ mm s^{-1}	$\delta/$ mm s^{-1}	$\Delta E_Q/$ mm s^{-1}
77	0.92	2.26	0.94	2.09	0.94	2.00
195	0.87	1.97	0.94	1.69	0.94	1.59
300	0.82	1.74	0.94	1.65	0.94	1.47

the quadrupole splitting lies outside of the error bars from the calibration study, which may be due to zero-point vibrational effects as discussed in the following.

The Mössbauer parameters of all structures in the generated ensembles at 77 K, 195 K and 300 K are shown in Fig. 3. For the isomer shift, no temperature dependence is observed in agreement with experiment. Strikingly, for the quadrupole splitting we not only observe the expected scatter around the positive value of the equilibrium structure, but in addition that some members of the ensemble have negative quadrupole splitting values. Moreover, the number of species with negative quadrupole splitting values increases with increasing temperature. We thus conclude that a key contributor to the temperature dependence of the quadrupole splitting are vibrational distortions that—crucially—lead to a swap in the sign of the quadrupole splitting. Note that experimentally, only the absolute value of the quadrupole splitting is routinely measured. Indeed, averaging the quadrupole splitting value over the ensemble, see Table 1 and Fig. 4, qualitatively reproduces the experimental trend of a decreasing quadrupole splitting with higher temperature. We also note that the agreement with the experimental quadrupole splitting value at low temperatures improves.

The observed changes in experimental and computed quadrupole splitting values can be traced back to the interlinked electronic and molecular structures. For an iron(II) high spin complex, one d orbital is doubly occupied. In the equilibrium structure, this is d_{xz}, see Fig. 2. When the structure is distorted along the normal coordinates, different orbitals can be stabilized, leading to different electronic configurations, hence different
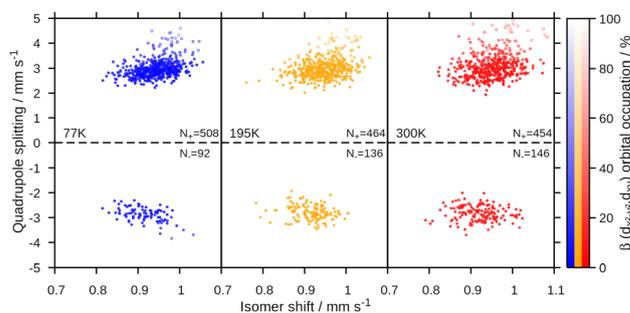

Fig. 2 Structure of the [Fe(TPP)(2-MeHIm)] complex[11] studied here alongside a qualitative molecular orbital diagram.

Fig. 3 Quadrupole splitting vs. isomer shift for all structures of the created ensembles at different temperatures. Labels indicate the temperature (left) and the number of structures with a positive/negative quadrupole splitting (right). The brightness of the points is defined by the sum of the $d_{x^2-y^2}(\beta)$ and $d_{xy}(\beta)$ orbital occupation.
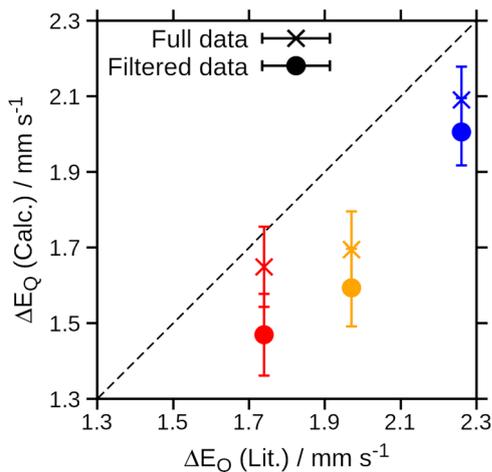
Fig. 4 Correlation of the experimental quadrupole splitting *versus* the computed quadrupole splitting averaged after Wigner sampling. Data points shown as crosses refer to the full data set; those shown as circles refer to the filtered data set. Error bars denote the statistical error obtained for the respective ensemble. The dashed line shows the ideal behaviour with a slope of 1.

charge distributions and thus ultimately different quadrupole splitting values. For [Fe(TPP)(2-MeHIm)], two relevant electronic configurations were identified. In one configuration, three electrons are distributed between the d_{xz} and d_{yz} orbitals, with the exact distribution depending on the deformation of the molecule and the mixing of those two orbitals. In the other configuration, the electrons are distributed between the $d_{x^2-y^2}$ and d_{xy} orbitals. This is represented in Fig. 3 by the brightness of the data points, which is scaled by the sum of the $d_{x^2-y^2}(\beta)$ and $d_{xy}(\beta)$ orbital occupation. The configuration with $(d_{x^2-y^2}, d_{xy})^3$ has an overall larger quadrupole splitting than that with the $(d_{xz}, d_{yz})^3$ configuration.

We note that filtering out the $(d_{xz}, d_{yz})^3$ configuration better reproduces the trend in the temperature dependence of the quadrupole splitting (see Table 1 and Fig. 4), albeit with a more pronounced discrepancy with the experimental values. This may indicate that on one hand, the vibrational component of the temperature effect is adequately captured for a single spin state. On the other hand, it may be the case that different spin states contribute in the experiment, either due to structural distortions caused by zero-point vibrations or electronic (near-)degeneracies, the ratio of which is likely not adequately represented by the single-determinant DFT calculations used here.

With the ensemble of vibrationally distorted structures in hand, the changes in Mössbauer parameters can be correlated to displacements along the normal coordinates of the [Fe(TPP)(2-MeHIm)] complex. Correlating these changes to individual normal coordinates does not deliver satisfactory results, see ESI,† supplemental file "Ensemble_Data.xlsx". Therefore, we turned to a multicomponent fitting procedure, in which the normal coordinates are used as basis functions to obtain collective motions that represent the observed changes. Methodological details are given in the ESI,† Methods S3 and S4.

For the isomer shift, a motion with a high correlation coefficient ($R^2 > 0.9$) was obtained. The fit parameters and nuclear movements are similar at all temperatures (see ESI,† Fig. S2).

For the quadrupole splitting, the R^2 value is lower (0.6183 to 0.6758) and the coefficients for each normal coordinate vary more strongly for the different temperatures, see Fig. S3 (ESI†). The resulting movement is similar at all temperatures. It comprises a strong out-of-plane movement of the iron ion combined with substantial stretching of the axial iron-nitrogen bond and weaker stretching of the in-plane iron-nitrogen bonds, see Fig. 5. This fits the expectations: the charge distribution in the out-of-plane direction changes strongly with this movement, thus converting its overall shape from oblate to prolate and *vice versa*, which hence results in the observed sign swap of the quadrupole splitting. The differences in the calculated nuclear movements for different temperatures lie mostly in the motion of the in-plane nitrogen atoms. Their motion is more difficult to capture due to the asymmetry around the iron nucleus introduced by the 2-MeHIm ligand and its CH_3 group close to the FeN_4 centre combined with the strong symmetry dependence of the quadrupole splitting.

To summarise, we have shown that a Wigner sampling approach generating a representative ensemble at different temperatures is indeed able to reproduce the vibrational temperature dependence of the quadrupole splitting. We identified as the root cause of the vibrational component of its temperature dependence that distortions lead to a swap in sign. A quantitative comparison with experimental data is likely hampered by different electronic spin ground states upon distortion incorrectly represented with DFT. Using a linear combination of normal modes, we have shown which collective nuclear movements are responsible for the observed changes. This provides a deeper understanding of the quadrupole splitting and its temperature dependence in general: the calculated movement explains how the charge distribution is converted from an oblate to a prolate shape and hence rationalises the sign swap for the quadrupole splitting.
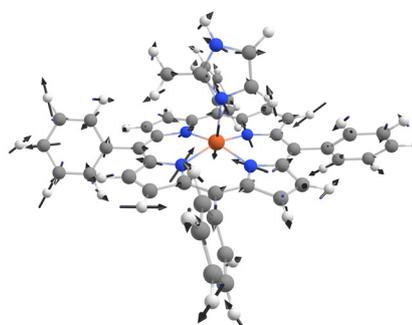
Fig. 5 Nuclear movement of the atoms in a [Fe(TPP)(2-MeHIm)] complex correlated to the quadrupole splitting calculated by a linear combination of normal modes at 77 K. The correlation coefficient is $R^2 = 0.6183$.

Data availability

The data supporting this article have been included as part of the ESI.† The computational codes used to generate the primary data are available free of charge for academic users.

Conflicts of interest

There are no conflicts to declare.

Notes and references

1 P. Gütlich, E. Bill and A. X. Trautwein, *Mössbauer Spectroscopy and Transition Metal Chemistry*, Springer Berlin Heidelberg, *Berlin, Heidelberg*, 2011.
2 E. Bill, *Practical Approaches to Biological Inorganic Chemistry*, Elsevier, 2020, pp. 201–228.
3 *Bioinorganic Chemistry*, ed. M. J. Clarke, Springer, Berlin and Heidelberg, 1991, vol. 78.
4 F. Neese, *Curr. Opin. Chem. Biol.*, 2003, **7**, 125–135.
5 M. D. Pluth and Z. J. Tonzetich, *Chem. Soc. Rev.*, 2020, **49**, 4070–4134.
6 H. T. Dong, C. J. White, B. Zhang, C. Krebs and N. Lehnert, *J. Am. Chem. Soc.*, 2018, **140**, 13429–13440.
7 D. Nam, J.-P. Bacik, R. L. Khade, M. C. Aguilera, Y. Wei, J. D. Villada, M. L. Neidig, Y. Zhang, N. Ando and R. Fasan, *Nat. Commun.*, 2023, **14**, 7985.
8 B. Boso, G. Lang and C. A. Reed, *J. Chem. Phys.*, 1983, **78**, 2561–2567.
9 C. Hu, J. An, B. C. Noll, C. E. Schulz and W. R. Scheidt, *Inorg. Chem.*, 2006, **45**, 4177–4185.
10 C. Hu, B. C. Noll, C. E. Schulz and W. R. Scheidt, *Inorg. Chem.*, 2018, **57**, 793–803.
11 J. P. Collman, J. L. Hoard, N. Kim, G. Lang and C. A. Reed, *J. Am. Chem. Soc.*, 1975, **97**, 2676–2681.
12 D. Dolphin, J. R. Sams, T. B. Tsin and K. L. Wong, *J. Am. Chem. Soc.*, 1976, **98**, 6970–6975.
13 M. L. Neidig, S. H. Carpenter, D. J. Curran, J. C. DeMuth, V. E. Fleischauer, T. E. Iannuzzi, P. G. N. Neate, J. D. Sears and N. J. Wolford, *Acc. Chem. Res.*, 2019, **52**, 140–150.
14 V. Schünemann, in *Modern Mössbauer Spectroscopy*, ed. Y. Yoshida and G. Langouche, Springer Singapore, Singapore, 2021, vol. 137 of Topics in Applied Physics, pp. 173–219.
15 C. Gallenkamp, U. I. Kramm and V. Krewald, *Chem. Commun.*, 2021, **57**, 859–862.
16 X. Li, K. Zhu, J. Pang, M. Tian, J. Liu, A. I. Rykov, M. Zheng, X. Wang, X. Zhu, Y. Huang, B. Liu, J. Wang, W. Yang and T. Zhang, *Appl. Catal., B*, 2018, **224**, 518–532.
17 Y. Lin, P. Liu, E. Velasco, G. Yao, Z. Tian, L. Zhang and L. Chen, *Adv. Mater.*, 2019, **31**, e1808193.
18 Y. Zeng, X. Li, J. Wang, M. T. Sougrati, Y. Huang, T. Zhang and B. Liu, *Chem. Catal.*, 2021, **1**, 1215–1233.
19 J. S. Bates, J. J. Martinez, M. N. Hall, A. A. Al-Omari, E. Murphy, Y. Zeng, F. Luo, M. Primbs, D. Menga, N. Bibent, M. T. Sougrati, F. E. Wagner, P. Atanassov, G. Wu, P. Strasser, T.-P. Fellinger, F. Jaouen, T. W. Root and S. S. Stahl, *J. Am. Chem. Soc.*, 2023, **145**, 26222–26237.
20 U. I. Koslowski, I. Abs-Wurmbach, S. Fiechter and P. Bogdanoff, *J. Phys. Chem. C*, 2008, **112**, 15356–15366.
21 U. I. Kramm, I. Herrmann-Geppert, S. Fiechter, G. Zehl, I. Zizak, I. Dorbandt, D. Schmeißer and P. Bogdanoff, *J. Mater. Chem. A*, 2014, **2**, 2663–2670.
22 U. I. Kramm, M. Lefèvre, N. Larouche, D. Schmeisser and J.-P. Dodelet, *J. Am. Chem. Soc.*, 2014, **136**, 978–985.
23 U. I. Kramm, I. Herrmann-Geppert, J. Behrends, K. Lips, S. Fiechter and P. Bogdanoff, *J. Am. Chem. Soc.*, 2016, **138**, 635–640.
24 U. I. Kramm, L. Ni and S. Wagner, *Adv. Mater.*, 2019, **31**, e1805623.
25 J. Li, S. Ghoshal, W. Liang, M.-T. Sougrati, F. Jaouen, B. Halevi, S. McKinney, G. McCool, C. Ma, X. Yuan, Z.-F. Ma, S. Mukerjee and Q. Jia, *Energy Environ. Sci.*, 2016, **9**, 2418–2432.
26 A. Zitolo, V. Goellner, V. Armel, M.-T. Sougrati, T. Mineva, L. Stievano, E. Fonda and F. Jaouen, *Nat. Mater.*, 2015, **14**, 937–942.
27 C. Gallenkamp, U. I. Kramm, J. Proppe and V. Krewald, *Int. J. Quantum Chem.*, 2021, **121**, e26394.
28 C. Gallenkamp, U. I. Kramm and V. Krewald, *JACS Au*, 2024, **4**, 940–950.
29 X. Li, C.-S. Cao, S.-F. Hung, Y.-R. Lu, W. Cai, A. I. Rykov, S. Miao, S. Xi, H. Yang, Z. Hu, J. Wang, J. Zhao, E. E. Alp, W. Xu, T.-S. Chan, H. Chen, Q. Xiong, H. Xiao, Y. Huang, J. Li, T. Zhang and B. Liu, *Chemistry*, 2020, **6**, 3440–3454.
30 J. Li, M. T. Sougrati, A. Zitolo, J. M. Ablett, I. C. Oğuz, T. Mineva, I. Matanovic, P. Atanassov, Y. Huang, I. Zenyuk, A. Di Cicco, K. Kumar, L. Dubau, F. Maillard, G. Dražić and F. Jaouen, *Nat. Catal.*, 2021, **4**, 10–19.
31 D. Menga, A. Guilherme Buzanich, F. Wagner and T.-P. Fellinger, *Angew. Chem.*, 2022, **61**, e202207089.
32 L. Ni, C. Gallenkamp, S. Paul, M. Kübler, P. Theis, S. Chabbra, K. Hofmann, E. Bill, A. Schnegg, B. Albert, V. Krewald and U. I. Kramm, *Adv. Energy Sustainability Res.*, 2021, **2**, 2000064.
33 L. Ni, C. Gallenkamp, S. Wagner, E. Bill, V. Krewald and U. I. Kramm, *J. Am. Chem. Soc.*, 2022, **144**, 16827–16840.
34 M. Pápai and G. Vankó, *J. Chem. Theory Comput.*, 2013, **9**, 5004–5020.
35 U. N. Morzan, D. J. Alonso de Armiño, N. O. Foglia, F. Ramírez, M. C. González Lebrero, D. A. Scherlis and D. A. Estrin, *Chem. Rev.*, 2018, **118**, 4071–4113.
36 P. R. Edwards, C. E. Johnson and R. J. P. Williams, *J. Chem. Phys.*, 1967, **47**, 2074–2082.
37 D. E. Freedman, W. H. Harman, T. D. Harris, G. J. Long, C. J. Chang and J. R. Long, *J. Am. Chem. Soc.*, 2010, **132**, 1224–1225.
38 M. T. Sougrati, V. Goellner, A. K. Schuppert, L. Stievano and F. Jaouen, *Catal. Today*, 2016, **262**, 110–120.
39 F. Jensen, *Introduction to Computational Chemistry*, John Wiley & Sons Incorporated, Newark, 1st edn, 2017.
40 A. L. Kholmetskii, T. Yarman, O. V. Missevitch and B. I. Rogozev, *Phys. Scr.*, 2009, **79**, 065007.
41 R. F. Wallis and C. G. Gazis, *Phys. Rev.*, 1962, **128**, 106–110.
42 C. M. Grunert, S. Reiman, H. Spiering, J. A. Kitchen, S. Brooker and P. Gütlich, *Angew. Chem.*, 2008, **120**, 3039–3041.
43 P. Gütlich and H. A. Goodwin, in *Spin Crossover in Transition Metal Compounds I*, ed. P. Gütlich and H. A. Goodwin, Springer Berlin Heidelberg, Berlin, Heidelberg, 2004, vol. 233 of Topics in Current Chemistry, pp. 1–47.
44 P. Gütlich, *Eur. J. Inorg. Chem.*, 2013, 581–591.
45 *Spin Crossover in Transition Metal Compounds I*, ed. P. Gütlich and H. A. Goodwin, Springer Berlin Heidelberg, Berlin, Heidelberg, 2004.
46 P. Gütlich and A. Hauser, *Coord. Chem. Rev.*, 1990, **97**, 1–22.
47 F.-L. Yang, B. Li, T. Hanajima, Y. Einaga, R.-B. Huang, L.-S. Zheng and J. Tao, *Dalton Trans.*, 2010, **39**, 2288–2292.
48 B. Weber, *Coord. Chem. Rev.*, 2009, **253**, 2432–2449.
49 R. W. Hogue, S. Singh and S. Brooker, *Chem. Soc. Rev.*, 2018, **47**, 7303–7338.
50 E. Wigner, *Phys. Rev.*, 1932, **40**, 749–759.
51 L. Sun and W. L. Hase, *J. Chem. Phys.*, 2010, **133**, 044313.
52 A. Šrut, B. J. Lear and V. Krewald, *Chem. Sci.*, 2023, **14**, 9213–9225.
53 F. Neese, *WIREs Comput. Mol. Sci.*, 2012, **2**, 73–78.
54 F. Neese, F. Wennmohs, D. Aravena, M. Atanasov, A. Auer, A. Alexander, U. Becker, G. Bistoni and D. Bykov, *et al.*, ORCA – An ab initio, DFT and semiempirical SCF-MO package – Version 5.0.3: Manual.
55 F. Neese, *WIREs Comput. Mol. Sci.*, 2022, **12**, 12753.
56 J. Tao, J. P. Perdew, V. N. Staroverov and G. E. Scuseria, *Phys. Rev. Lett.*, 2003, **91**, 146401.
57 V. N. Staroverov, G. E. Scuseria, J. Tao and J. P. Perdew, *J. Chem. Phys.*, 2003, **119**, 12129–12137.
58 F. Weigend and R. Ahlrichs, *Phys. Chem. Chem. Phys.*, 2005, **7**, 3297–3305.
59 S. Mai, P. Marquetand and L. Gonzalez, *WIREs Comput. Mol. Sci.*, 2018, **8**, e1370.
60 S. Mai, D. Avagliano, M. Heindl, P. Marquetand, M. F. S. J. Menger, M. Oppel, F. Plasser, S. Polonius, M. Ruckenbauer, Y. Shu, D. G. Truhlar, L. Zhang, P. Zobel and L. Gonzalez, *SHARC3.0: Surface Hopping Including Arbitrary Couplings—Program Package for Non-Adiabatic Dynamics*, https://sharc-md.org/, 2023.
61 J. P. Zobel, O. S. Bokareva, P. Zimmer, C. Wölper, M. Bauer and L. González, *Inorg. Chem.*, 2020, **59**, 14666–14678.
62 A. D. Becke, *J. Chem. Phys.*, 1993, **98**, 1372–1377.
63 F. Neese, *Inorg. Chim. Acta*, 2002, **337**, 181–192.
64 M. Radoń, in *Computational Chemistry*, ed. R. van Eldik and R. Puchta, Elsevier, Amsterdam, 2019, vol. 73 of Advances in Inorganic Chemistry, pp. 221–264.
65 M. Radoń, *J. Chem. Theory Comput.*, 2014, **10**, 2306–2321.
66 M. Swart, *J. Chem. Theory Comput.*, 2008, **4**, 2057–2066.
67 G. Li Manni, D. Kats, D. P. Tew and A. Alavi, *J. Chem. Theory Comput.*, 2019, **15**, 1492–1497.